ORIGINAL ARTICLE

Human duodenal organoid-derived monolayers serve as a suitable barrier model for duodenal tissue

Franziska Weiß[1] | **David Holthaus**[2] | **Martin Kraft**[2] | **Christian Klotz**[2] |
Martina Schneemann[1] | **Jörg D. Schulzke**[1] | **Susanne M. Krug**[1]

[1]Clinical Physiology/Nutritional Medicine, Charité – Universitätsmedizin Berlin, CBF, Berlin, Germany

[2]Department of Infectious Diseases, Unit 16 Mycotic and Parasitic Agents and Mycobacteria, Robert Koch-Institute, Berlin, Germany

Correspondence
Susanne M. Krug, Clinical Physiology/Nutritional Medicine, Charité – Universitätsmedizin Berlin, CBF, Berlin 12203 Germany.
Email: Susanne.m.krug@charite.de

Current address
David Holthaus, Laboratory of Infection Oncology, Institute of Clinical Molecular Biology, University Hospital Schleswig-Holstein, Kiel, Germany

Abstract

Usually, duodenal barriers are investigated using intestinal cell lines like Caco-2, which in contrast to native tissue are limited in cell-type representation. Organoids can consist of all intestinal cell types and are supposed to better reflect the *in vivo* situation. Growing three-dimensionally, with the apical side facing the lumen, application of typical physiological techniques to analyze the barrier is difficult. Organoid-derived monolayers (ODMs) were developed to overcome this. After optimizing culturing conditions, ODMs were characterized and compared to Caco-2 and duodenal tissue. Tight junction composition and appearance were analyzed, and electrophysiological barrier properties, like paracellular and transcellular barrier function and macromolecule permeability, were evaluated. Furthermore, transcriptomic data were analyzed. ODMs had tight junction protein expression and paracellular barrier properties much more resembling the originating tissue than Caco-2. Transcellular barrier was similar between ODMs and native tissue but was increased in Caco-2. Transcriptomic data showed that Caco-2 expressed fewer solute carriers than ODMs and native tissue. In conclusion, while Caco-2 cells differ mostly in transcellular properties, ODMs reflect trans- and paracellular properties of the originating tissue. If cultured under optimized conditions, ODMs possess reproducible functionality, and the variety of different cell types makes them a suitable model for human tissue-specific investigations.

KEYWORDS
barrier function, Caco-2 cells, duodenum, organoids, tight junction

INTRODUCTION

The gastrointestinal tract is the main place of solute absorption and secretion and forms the first barrier against microbial and viral pathogen assault. The complex morphology of the small intestine is specialized in the different small intestinal segments, including the crypts of Lieberkühn, as well as the villus, that contain several cell types to maintain epithelial homeostasis and regeneration. Although recently many different subtypes have been described,[1] four major differentiated cell types perform the function of the small intestine: absorptive enterocytes, mucus-secreting goblet cells, hormone-secreting enteroendocrine cells, and antimicrobial peptide-secreting Paneth cells.[2] These cell types are produced by self-renewing stem cells located in the crypt base and migrate in coherent bands along the crypt–villus axis; however, Paneth cells return to the crypt bottom.[3]

Functionality of the small intestine becomes disturbed in a variety of diseases, including inflammatorily driven pathologies like ulcerative colitis, Crohn's disease, or celiac disease, congenital diseases as lactose

intolerance, and cancer. Thus, to study the properties and regulation of the small intestine in health and disease, sufficient models are needed. For decades, the two main models were animal intestine (*in vivo* or *ex vivo*) and transformed cancer-derived intestinal cell lines.

Animal models, though possessing the real morphology and all cell types, not necessarily mimic the exact conditions and reactions of human tissue well; they are costly, labor-intensive, and not suitable for high-throughput procedures. Additionally, for ethical reasons, there is an impetus to reduce or refrain from animal experiments if there are valid alternatives.[4]

Commonly used cell lines include T84 and Caco-2, which have been used as *in vitro* models for human small intestinal epithelia as they reflect intestinal permeability and membrane transport.[5,6] However, they do not originate from small intestinal tissue, but colon carcinoma and lung metastases, which also means that they are mutated with lots of defects (e.g., immune-regulating and apoptosis-inducing signals), which may not be problematic for general physiological studies, but for molecular biological attempts or—omics studies. In addition, they vary in their properties between different laboratories, may change their genetics and biological behavior with time, which results in changed proliferation, barrier properties, metabolic activity, and expression profiles of receptor and transport proteins.[7,8] Furthermore, they lack intestinal segment-specificity and do not possess the morphology of the intestine, as on the one hand, they contain only one of the cell types present in the intestine, and on the other hand, they do not form crypt-villus structures as they grow as flat monolayers.

Attempts to cultivate primary cultures from intestinal tissue as monolayers comparable to immortalized cell lines for longer times have not been possible due to rapid loss of proliferation and renewal.[9] In 2009, Sato and colleagues managed to culture murine intestinal stem cells long-term and found that these cultures consist of stem cells that further have the ability to differentiate into all tissue-specific cell types.[10] These so-called organoids can derive from adult stem cells located in the crypt base and, when cultured under conditions of the tissue-specific stem cell niche, can recapitulate the capacity for self-renewal and differentiation of the tissue of origin.[11] Due to those properties, organoids became a highly appreciated model for the epithelial layer of the intestine and are suitable for the investigation of a variety of gastrointestinal research topics like cancer development,[12] tissue homeostasis,[13] infectious diseases,[14,15] inflammatory bowel disease,[16] and barrier research.[17]

However, a drawback to use organoids for the investigation on the epithelial barrier is that organoids, normally seeded in extra cellular matrix, grow three dimensionally with the apical side facing the lumen,[10,18] making it difficult to measure, for example, transepithelial resistance (TER), or to quantify permeabilities for ions, small or macromolecular solutes, or in general to access and stimulate the epithelium from the apical side.

To overcome these problems, researchers have begun growing monolayers derived from organoids (organoid-derived monolayer; ODM) on filter inserts giving access to both the basal and apical sides of what are primary epithelial cells,[19–21] allowing to measure TER and tracer fluxes, or mount them in Ussing chambers to perform an in-depth analysis of the epithelial barrier, as is known for tissue samples or

common cell lines.[22] At the same time, ODMs benefit from the advantages of organoids, such as the composition of different cell types, their great genetical stability, and the much higher availability compared to tissue samples. However, this also indicates that reproducible properties are an essential criterium that must be established to give a reliable model. First, efforts to harmonize protocols for different species have been undertaken by our group, as differences may lead to changes in barrier properties and behavior.[23,24]

One main factor representing the barrier properties is the tight junction (TJ), which is determining the epithelial paracellular barrier. It is composed of a variety of TJ proteins, including the family of claudins,[25] TJ-associated MARVEL proteins,[26] angulins,[27] and many nonmembrane scaffold-proteins like ZO-1.[28] Different cell types of the intestine have been shown to possess different TJ protein expression levels, and thus, might differently affect the barrier properties,[29] underlining the relevance of reproducible conditions to make ODMs a good model of the intestine.

In this work, we compared human duodenal tissue, ODMs, and Caco-2 cells regarding their barrier properties, which are based on TJs. We show that human duodenal ODMs reflect human duodenal tissue properties better than the commonly used Caco-2 cells, as evaluated for barrier function and protein expression. We conclude that ODMs serve as a good model for human intestinal barrier properties.

METHODS

Patient samples

The usage of human duodenum biopsies from healthy controls was approved by the ethical committee of the Charité Berlin (#EA4-015-13). Tissue specimens were either used for barrier characterization in Ussing chambers, for isolation of intestinal crypts, or for freeze fracture electron microscopy.

Crypt isolation

Crypt isolation was based on the protocol for corpus glands from Bartfeld *et al.*[30] Tissues were washed in cold PBS (Gibco, ThermoFisher, Rockford, IL, USA) and cleaned from connective, muscle, and adipose tissue with forceps. Epithelial tissue was cut in small pieces and transferred in a 50 ml falcon tube filled with PBS. Pieces were washed by resuspending them in PBS with a 0.1% BSA (Sigma-Aldrich, Steinheim, GER)-coated 10 ml serological pipette for several times until the supernatant was clear. After the last washing step, the supernatant was removed, and epithelial pieces were digested by 5 ml 2.5 mM EDTA in PBS for 5–10 min at room temperature. Afterwards, pieces were transferred with as few liquid as possible on a petri dish and a microscope slide was placed on top of the pieces to finally press the crypts out of the tissue, success was indicated by a cloudy appearance around the tissue pieces. Cover slide and petri dish were rinsed with Advanced Dulbecco's modified Eagle medium (DMEM)/F12 (Gibco) supplemented with 10 mmol/L HEPES (Gibco), 1× GlutaMax (Gibco)

TABLE 1 Organoid and ODM media composition

Protocol [reference]	L-WRN CM[31]	Rspo1 CM[32] (20%)	Noggin CM[33] (10%)	EGF (50 ng/ml)	NAC (1 mM)	NIC (10 mM)	SB-202190 (1 μM)	A83-01 (500 nM)	Y-27632 (10 μM)	DAPT (1 μM)	FCS(20%)
WERN[23]	50%	X	X	X	X	X	X	X	Initially		
Standard (SM)[23]		X	X	X	X	X			Initially		
DAPT[34]	25%	X	X	X	X			X		X	
ENA[19]		X	X	X				X			
FCS[20,35,36]	5%								X		20%

Note: All media were based on Advanced Dulbecco's modified Eagle medium (DMEM)/F12 (Gibco) with 10 mmol/L HEPES (Gibco), 1× GlutaMax (Gibco) and 100 U/ml penicillin, 100 μg/ml streptomycin (Corning) (AD+++) supplemented with 1× B27 (Gibco) and 1× N2 (Gibco). L-WRN conditioned medium (CM); Rspo1-CM and Noggin-CM (produced from stable transfected HEK293 cells (ATTC) with Rspo1 or Noggin); human recombinant epithelial growth factor (EGF, Peprotech, Hamburg, Germany); *N*-acetylcysteine (NAC, Sigma-Aldrich), nicotinamide (NIC, Sigma-Aldrich); p38 inhibitor (SB 202190, Stemcell, US); TGF-β inhibitor (A83-01, Stemgent,Cambridge, MA, USA); Rho-K inhibitor (Y-27632, Tocris); Notch inhibitor DAPT (Sigma-Aldrich); fetal calf serum (FCS, Gibco).

and 1% 100 U/ml penicillin, 100 mg/ml streptomycin (Corning, NY, USA) (AD+++) to collect tissue pieces and isolated crypts. Suspension was transferred into a 15 ml falcon tube and stored on ice until the tissue pieces were settled. Supernatants containing epithelial crypts were transferred to a new falcon tube and pelleted at $500 \times g$ (4°C) for 5 min. The crypt pellet was resuspended in Matrigel (50 μl/well, 354230, BD Bioscience/Corning) and seeded on a prewarmed 24 well plate (TPP/Merck, Darmstadt, GER). The plate was stored for 15–30 min at 37°C to let the Matrigel solidify before it was overlaid with WERN medium (Ref. 23, Table 1) supplemented with 10 μM Rho-K inhibitor (Y-27632, Tocris, Bristol, UK).

Duodenal organoid culture

For organoid culture, medium was changed every other day and organoids were passaged by mechanical destruction once a week. For that, medium was replaced by 500 μl cold AD+++ and Matrigel was dissolved by resuspending with a 1 ml Pipette. Cell suspension was transferred in a 15 ml falcon tube and organoids were broken up by resuspending with a 21G Needle coated with 0.1% BSA. Organoid pieces were pelleted at $300 \times g$ for 5 min at 4°C. The organoid pellet was resuspended in Matrigel (50 μl/well, 354230 BD Bioscience/Corning) and seeded on a prewarmed 24 well plate. The plate was stored for 15–30 min at 37°C to let the Matrigel solidify before it was overlaid with WERN medium. Y-27632 was only added after splitting and removed after 24 h.

Seeding of organoids-derived monolayers

To generate ODMs, 3D organoids were broken into pieces as described above and the organoid pellet was incubated for 5–10 min at 37°C in TrypLE Express (Gibco). To obtain single cells, further mechanical destruction, using a 21G needle, was necessary. Cells were counted, and TrypLE Express was inactivated by diluting with AD+++. Cells

were pelleted by centrifuging at $500 \times g$ at 4°C for 5 min and seeded on Matrigel-coated PCF filters (Merck Millipore, Tullagreen, Carrigtwohill, IRL) ($0.5–1 \times 10^6$ cells/filter). For coating, 150 μl of a 1:50 mixture of Matrigel and ice cold Advanced DMEM/F12 was added on each filter. Filters were incubated for at least 30 min at 37°C. Before adding the cell suspension, remaining advanced DMEM/F12 was removed. For differentiation, ODMs were cultured with differentiation media standard medium (SM) (Ref. 23, Table 1). ODMs were used for experiments after reaching confluency and stable TER, normally between 8 and 10 days after seeding. For the air–liquid interface (ALI) culture, cells were seeded as described above and apical medium was withdrawn as soon as monolayers reached confluency.

Reverse transcriptase quantitative polymerase chain reaction

For reverse transcriptase quantitative polymerase chain reaction (RT-qPCR), medium was aspirated from ODMs, and cells were directly lysed with 2×300 μl TriReagent (Zymo, Cat. No. R2050-1-200). RNA was extracted using the Directzol-RNA Microprep (Zymo, Cat. No. R2062) kit, including an on-column DNase I digest following manufacturer's instructions. RNA was quantified using 260/280 nm absorption measurements using a NanoQuant plate on an Infinite M200 Pro reader (both Tecan). Five hundred nanograms of RNA were reversely transcribed using the High-Capacity RNA-to-cDNA Kit (Applied Biosystems, Cat. No. 4387406) following the manufacturer's instructions. RT-qPCR was performed using 10 ng cDNA per reaction on a CFX96 system with C1000 Cycler (both Biorad) using the Maxima SYBR Green qPCR Master Mix (2×, Thermo Fisher, Cat. No. K0251). Cycling included an initial 10 min enzyme activation step at 95°C, followed by 40 cycles of 20 s at 95°C, 30 s at 60°C, and 20 s at 72°C. Melting curve analysis was performed to verify amplicon specificity. Relative expression was calculated using the $\Delta\Delta C_T$ method. Primer sequences are included in Table S1.

Caco-2 cells

Caco-2 cells (ATCC HBT-37) were cultured at 37°C and 5% CO_2 with Earl's Minimal Essential Medium + GlutaMax (41090-028 Gibco) supplemented with 15% (v/v) fetal calf serum (FCS, Gibco) and 100 U/ml penicillin, 100 μg/ml streptomycin (Corning). For experiments, cells were seeded on PCF filters (0.4 μm pore size, area 0.6 cm^2; Merck Millipore) and grown for 3 weeks to differentiate to a small intestinal cell-like phenotype.[37] Regular TER measurements were performed to confirm sufficient differentiation of the cell layers.

Immunofluorescent staining of ODMs

To check for several TJ protein localizations, ODMs were fixed in 2% PFA for 20 min at room temperature and permeabilized with 0.2% Triton X-100 in PBS$^{+/+}$ for 10 min, blocked with 5% goat serum and 5% BSA in PBS$^{+/+}$, and incubated at 4°C over night with primary antibodies, followed by incubation with secondary antibodies for 1 h at 37°C before staining for ZO-1 (conjugated AB; 1:500) and nuclei staining with DAPI (1:1000). All used antibody concentrations and sources can be found in Table S2. Images were obtained using a confocal laser-scanning microscope (LSM 780, Carl Zeiss AG, Jena, Germany) with excitation wavelengths of 488, 543, and 633 nm.

Western blots

To compare protein expression, Caco-2 and ODMs on filters were washed with ice-cold phosphate-buffered saline and scraped off the filter support. Caco-2, ODMs, and tissue samples were incubated on ice in membrane lysis buffer (1 M Tris-Cl pH 7.4, 1 M MgCl$_2$, 0.5 M ethylenediaminetetraacetic acid, 0.5 M ethylene glycol tetra acetic acid, and protease inhibitors), homogenized with an insulin needle, and centrifuged at $200 \times g$ for 5 min at 4°C. Membrane proteins were pelleted by a long centrifugation at $42{,}100 \times g$ for 30 min at 4°C. Protein pellet was resuspended in total lysis buffer (10 mM Tris-Cl pH 7.5, 150 mM NaCl, 0.5% Triton X-100, 0.1% SDS, and protease inhibitors).

Membrane proteins (8 μg of Caco-2 lysate, 3 μg of ODM's lysate, and 20–30 μg of tissue) were loaded on 12.5% sodium dodecyl sulphate-polyacrylamide gel, separated at 100 V, and transferred to PVDF membranes (Perkin Elmer, Rodgau, Germany). For immunodetection, membranes were incubated in blocking solution (1% polyvinylpyrrolidone-40, 0.5% Tween) for 1 h and incubated over night with primary antibodies (Table S2). Membranes were washed and incubated for 2 h at room temperature with peroxidase-coupled secondary antibodies before detection using chemiluminescence, SuperSignal West Pico PLUS (Thermo Fisher). Signals were detected using Fusion FX (Vilber Lourmat), and densitometric analysis was done using AIDA (Elysia).

Transcriptomic analysis

Comparison of the qualitative expression of typical transporter genes between Caco-2, tissue, ODMs, and organoids was performed using the following data sets, available at Gene Expression Omnibus (GEO): GSE164334,[38] GSE156453,[39] GSE127938,[40] GSE167286,[41] GSE163706, and[42] GSE160695;[43] and one data set from Ma'ayeh et al.[44] and our own data.[15] Since these data were obtained using different methods (RNAseq and DNA microarray), they were only qualitatively evaluated according to whether transporters were reported to be expressed. RNAseq data and DNA microarray data were normalized by the respective authors or according to the manufacturer's guidelines.[43] This evaluation was summarized and visualized using Prism 9.1 software (GraphPad).

Freeze fracture electron microscopy

Freeze fracture electron microscopy was performed as previously described.[45] Briefly, ODMs were fixed with phosphate-buffered glutaraldehyde (2%). Preparations were incubated in 10% (v/v) and then in 30% (v/v) glycerol, and finally frozen in liquid nitrogen-cooled Freon 22. Cells were fractured at −100°C and shadowed with platinum and carbon in a vacuum evaporator (Denton DV-502). Replicas were bleached with sodium hypochloride, picked up on grids (Ted Pella Inc.), and analyzed with a video-equipped Zeiss 902 electron microscope (Carl Zeiss AG; Olympus iTEM Veleta).

Morphometrical analysis was performed at a final magnification of 51,000×. Vertical grid lines were drawn at 200 nm intervals perpendicular to the most apical TJ strand.[46] Number of strands horizontally oriented within the main TJ meshwork was counted at intersections with grid lines. The distance between the most apical and contra-apical strand was measured as the meshwork depth. Strand discontinuities within the main compact TJ meshwork of >20 nm were defined as breaks and their number is given per μm length of horizontally oriented strands. Strand formation was noted as particle type or continuous type.

Paracellular flux measurements

Flux studies were performed in Ussing chambers under short-circuit conditions. For flux measurements, after apical addition of FITC-labeled and dialyzed 4 kDa dextran (0.4 mM, TdB Consultancy, Sweden) together with basolateral addition of unlabeled dextran of the same size (0.4 mM, Serva, Heidelberg, Germany), basolateral samples were taken at 0, 30, 60, 90, and 120 min. Tracer fluxes and apparent permeabilities were calculated from the amount of FITC-dextran in the basolateral compartment measured fluorometrically (Tecan Infinite M200, Tecan, Switzerland).

Electrogenic chloride secretion

For measuring electrogenic Cl^- secretion, ODMs were stimulated by prostaglandin E2 (10^{-6} mol/l, serosal side) and theophylline (10^{-2} mol/l, both sides). The increase in I_{SC} (ΔI_{SC}) was measured thereafter. After reaching steady state, the effect of theophylline and prostaglandin E2 was antagonized by bumetanide (10 μmol/l, serosal side) and the decrease in I_{SC} was measured.

One-path and two-path impedance spectroscopy

Impedance spectroscopy was performed based on a model describing the epithelial resistance, R^{epi}, as a parallel circuit consisting of the transcellular resistance, R^{trans}, and the paracellular resistance, R^{para}. The subepithelial resistance, R^{sub}, is in series to R^{epi} and, in cell cultures, is caused by the filter support. After application of alternating current (35 μA/cm^2, frequency range 1.3–65 kHz), changes in tissue voltage were detected by phase-sensitive amplifiers (402 frequency response analyzer, Beran Instruments; 1286 electrochemical interface; Solartron Schlumberger). Complex impedance values (Z_{real}, $Z_{imaginary}$) were calculated and plotted in a Nyquist diagram. Because of the frequency-dependent electrical characteristics of the epithelium, R^t (= TER) could be obtained at minimum and R^{sub} at maximum frequency, and R^{epi} was calculated using $R^{epi} = R^t - R^{sub}$ (one-path impedance spectroscopy). R^{trans} and R^{para} were determined from experiments in which impedance spectra and fluxes of fluorescein as a paracellular marker substance were obtained before and after chelating extracellular Ca^{2+} with EGTA (two-path impedance spectroscopy), which caused TJs to partly open and increase fluorescein flux.[47]

Statistical analysis

MS ECXEL (Microsoft) or Prism 9.1 software (GraphPad) was used for analysis. If not stated otherwise, data are expressed as mean values ± standard error of the mean (SEM), indicating n as the number of single measurements. Statistical analysis was performed using Student's t-test with Bonferroni–Holm correction for multiple testing or one-way ANOVA with Dunnett correction for multiple comparison. $p < 0.05$ was considered significant (*$p < 0.05$, **$p < 0.01$, ***$p < 0.001$).

RESULTS

Optimization of culture conditions and validation of the ODMs

To compare ODMs and Caco-2 cells in their ability to reflect the barrier properties of duodenal tissue, the appropriate conditions of the ODM culture had to be found. Several research groups started to work with ODMs and as many different media compositions are postulated. In this study, four different media were tested for their stability in the TER and their cell composition. Single cells derived from organoids were seeded on PCF filters with SM (Table 1). Medium was changed every other day and monolayers reached a plateau of TER after 7–8 days. On day 8, the medium was changed to DAPT (Notch inhibitor N-[N-(3,5-difluorphenacetyl)-L-alanyl]-S-phenylglycin-tert-butylester),[34] ENA (epidermal growth factor + Noggin + A83-01),[19] and FCS (fetal calf serum)[20,35,36] for ODMs or culture continued with SM (see composition of the different media in Table 1). TER was measured daily from day 3 to day 11 and increased to 200 $\Omega \cdot cm^2$ by day 8 after seeding and remained stable for SM and ENA until day 11, while the TER of filters with DAPT decreased to 120 $\Omega \cdot cm^2$ on day 11 (Figure 1A). Under FCS conditions, TER dramatically decreased to below 100 $\Omega \cdot cm^2$ as early as day 9, and by day 11 the TER equaled that of empty filters.

ODMs' transcriptional data were normalized to the SM/SM composition (Figure 1B), in comparison, SM/DAPT and SM/ENA ODMs seemed to be more differentiated as they had a significantly lower expression of the main stem cell marker Leucine-rich repeat-containing G-protein coupled receptor 5 (*LGR5*) and significantly higher expressions for the enterocyte markers fatty acid-binding protein (*FABP2*) and sucrase-isomaltase (*SI*) and goblet cell markers mucin 2 (*MUC2*) and trefoil factor 3 (*TFF3*). The expressions of other cell markers for stem cells olfactomedin 4 (*OLFM4*), for enterocytes sodium/glucose-cotransporter 1 (*SGLT1/SLC5A1*) and peptide transporter 1 (*PEPT1/SLC15A1*) and progenitor cells atonal BHLH transcription factor 1 (*ATHO1*), SRY-box transcription factor 9 (*SOX9*), and delta-like ligand 4 (*DLL4*), as well as for Paneth cells lysozyme (*LYZ*), were comparable between SM/SM, SM/DAPT, and SM/ENA ODMs. The SM/FCS condition had a significant lower expression of LGR5, too, but in contrast, a significantly lower expression of *TFF3*, *PEPT1*, and *LYZ*. Conversely, the notch pathway ligand *DLL4* was significantly higher in SM/FCS. The enteroendocrine marker chromogranin A (*CHGA*) could not be detected for all four conditions, which is in line with previous publications using the medium conditions.[15,23]

Due to these results, the SM/SM or the SM/ENA conditions were found to be the most suitable, as both lead to a stable TER, and the markers for stem cells, Paneth cells, goblet cells, and enterocytes were detected. In addition, SM/SM has been described to not only work for human duodenal tissue but also for mouse, chicken, and pig ODMs.[23] Moreover, it was also suitable for infection studies, as shown for *Giardia duodenalis* infection.[15] Therefore, further experiments were performed using SM/SM conditions.

Next, the expression and localization of TJ proteins in ODMs under SM/SM conditions was confirmed by immunofluorescence staining (Figure 2 and Figure S1). Typically, in intestinal duodenum, expressed members of the claudin (CLDN) family were found, including CLDN1, CLDN2, CLDN3, CLDN4, CLDN7, and CLDN15. Furthermore, the TAMP proteins occludin (OCLN) and tricellulin (TRIC), as well as lipolysis-stimulated lipoprotein receptor (LSR), were expressed in duodenal ODMs. Moreover, TJ proteins were located apically within the cell membranes of the monolayer, and TRIC was specifically expressed at the tricellular corners of the epithelial cells.

These results showed that the chosen ODM system was a suitable model to investigate the duodenal TJ barrier, as they had stable TER
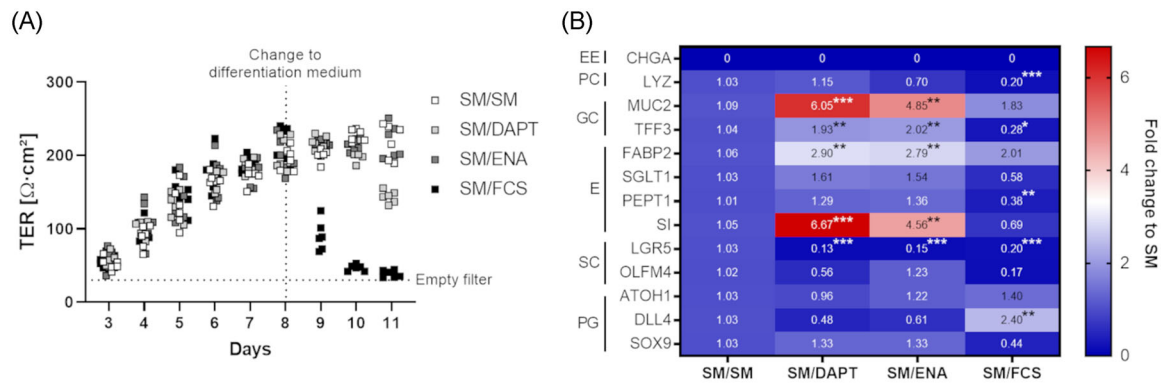
FIGURE 1 TER and RT-qPCR data comparing different culture conditions: (A) TER values of ODMs from day 3 to day 11 after seeding. Single cells derived from organoids were seeded on permeable cell culture supports and cultured in standard medium (SM) until day 8. Then, medium was changed either to DAPT, ENA, or FCS medium or maintained in SM ($n = 6$). (B) After day 11, RNA was extracted from ODMs and RT-qPCR was performed for the detection of different epithelial cell makers. Dark blue represents decreased expression and red represents increased expression. ($n \geq 5$; data are shown as mean; $^*p < 0.05$, $^{**}p < 0.01$, $^{***}p < 0.001$). Abbreviations: E, enterocytes; EE, enteroendocrine cells; GC, Goblet cells; PC, Paneth cells; PG, progenitor cells; SC, stem cells
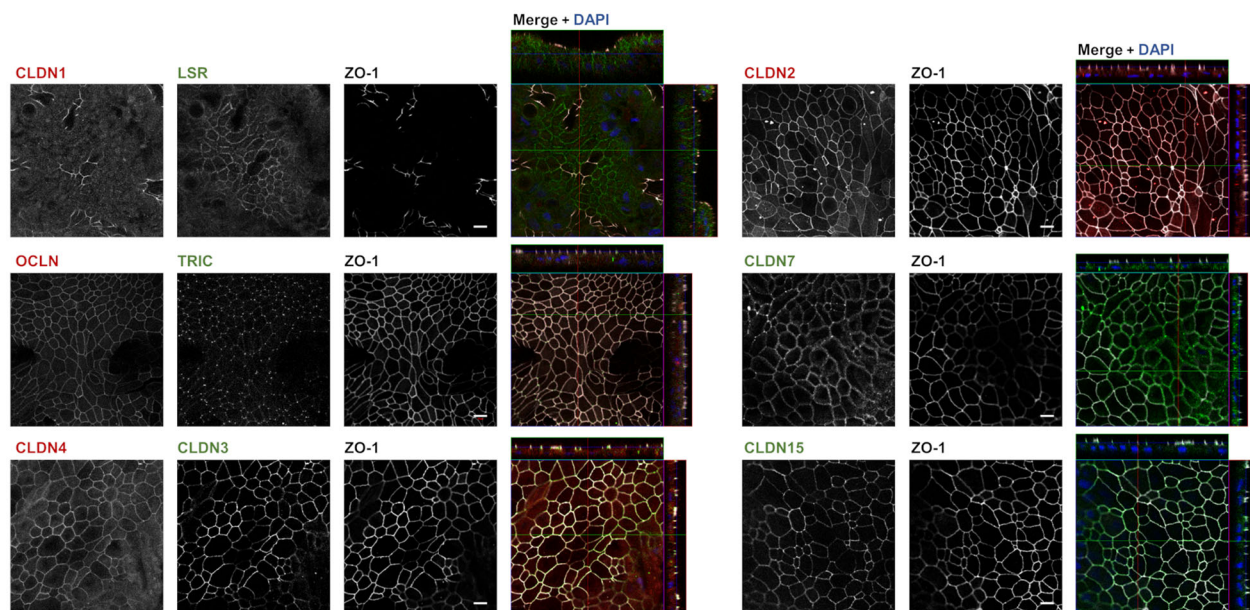

FIGURE 2 Expression and localization of TJ proteins. Representative immunofluorescence images of a duodenal organoid culture (CBF1) 10 days after seeding on permeable cell culture supports cultured with SM medium. For better visibility, signal intensities were increased, and single panels are shown in white. In merge images, the counterstaining ZO-1 (white), nuclei (blue), and the detected TJ proteins (green or red) are shown. The vast expression of TJ proteins indicates well polarization of ODMs and presence of a continuously expressed TJ barrier. Bar = 10 μm

values, were composed of different intestinal cell types, and expressed TJ proteins that were expected in duodenal tissue.

Comparison of expression profiles of duodenal tissue, ODMs, and Caco-2 cells

First, ODMs under SM/SM conditions and the commonly used Caco-2 cell line were compared to tissue samples regarding their composition of TJ proteins by western blotting. For that, protein was extracted from either tissue samples, 3-week-old Caco-2, or 10-day-old ODMs, both grown on filter supports. Protein concentration was normalized to Cytokeratin 19 (CK19) expression, which is a marker for epithelial cells. Usage of this marker was necessary because Caco-2 cells and ODMs did not contain subepithelial tissues, which were present in the duodenal tissue samples and needed to be considered as additional protein fraction. Accordingly, this led to loading of different amounts of protein to make the epithelial proportions represented by CK19
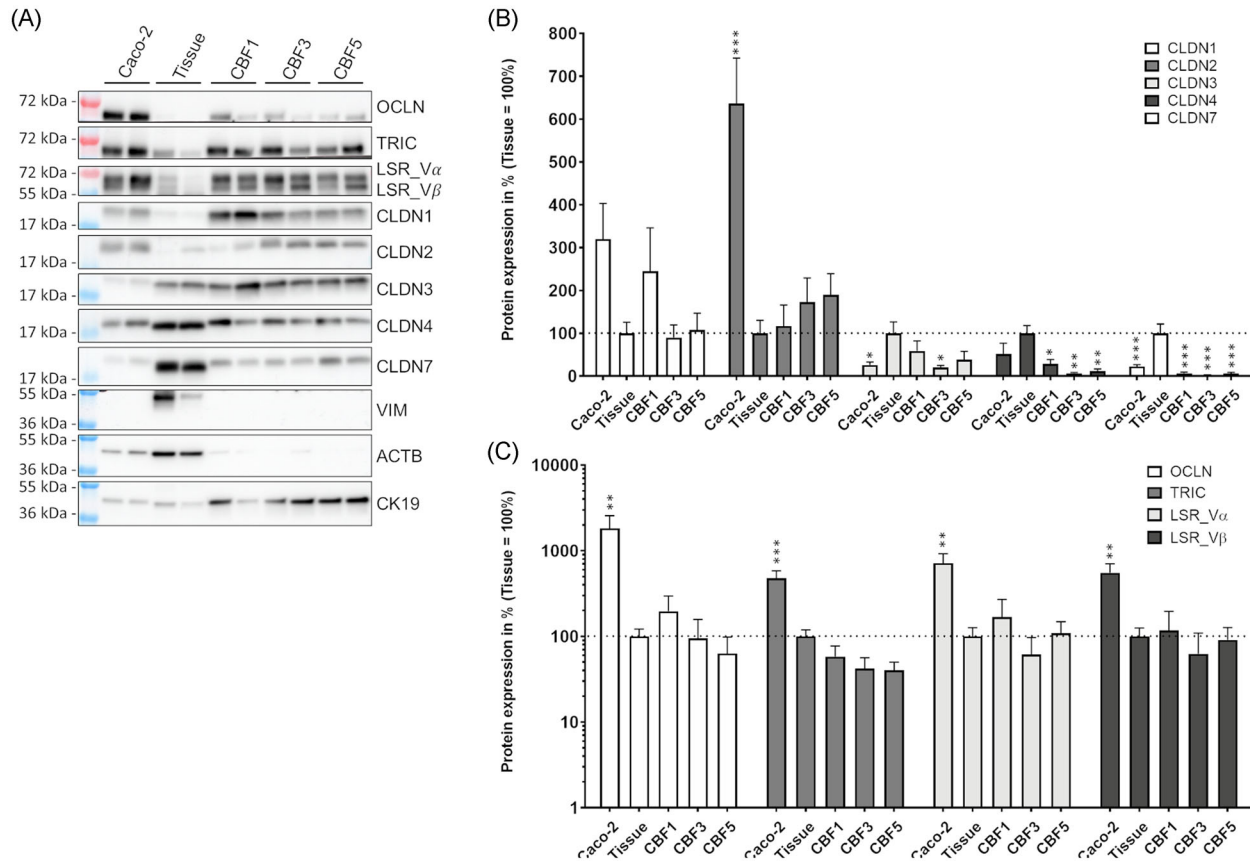
FIGURE 3 Comparison of TJ protein expression between duodenum tissue, ODMs, and Caco-2 cells. Proteins were isolated 10 days post seeding of ODMs and 21 days post seeding of Caco-2 cells. (A) Representative western blots showing the expression of several TJ proteins, including OCLN, TRIC, LSR variant α and variant β, CLDN1, CLDN2, CLDN3, CLDN4, CLDN5, CLDN7, as well as the commonly used housekeeping gene ACTB, the mesenchymal marker VIM, and the marker for epithelial cells CK19. (B) and (C) Quantification of TJ proteins. VIM is shown to emphasize that tissue samples not only consist of epithelium but also surrounding tissue, therefore, ACTB was not used as housekeeping gene but CK19. For quantification, densitometric intensities were normalized to CK19, and mean value of tissue samples was set to 100% (values are shown as mean ± SEM; *$p < 0.05$, **$p < 0.01$, ***$p < 0.001$)

as uniform as possible (Figure 3A). CLDN1 (22 kDa) was expressed similarly between native tissue and the two barrier models. However, Caco-2 cells and the organoid line CBF3 had a lower expression of CLDN3 (22 kDa). Furthermore, the amount of CLDN4 (22 kDa) was lower in all three organoid lines than in the tissue, and CLDN7 (22 kDa) expression was more abundant in native tissue compared to all other samples (Figure 3B). In contrast, the expressions of CLDN2 (22–23 kDa), the TAMPs OCLN (65 kDa), and TRIC (65 kDa), as well as LSR (splice variants α 68 kDa and β 56 kDa[48]) in ODMs, were very similar to that of the tissue sample, while Caco-2 cells had a higher expression of those proteins (Figure 3C). Furthermore, ODMs reflected individual properties of the donors as the TJ protein expression slightly differed between the organoid lines. CBF1 had the highest protein expression and the CBF3 line the lowest.

Besides analyzing the TJ protein expression profiles, the expressions of solute carrier (SLC) transporter genes in Caco-2, tissue, organoids, and ODMs were compared using data available in the literature and own transcriptomic data (Figure 4 and Table S3). This

analysis revealed that 218 SLCs were expressed in all duodenal tissue samples analyzed. Of these, ODMs and organoids expressed 191–214 and 188–205, respectively (Figure 4A). Although some Caco-2 cell samples expressed 208 of the 218 SLCs expressed in tissue, other samples expressed only 152 of 218 SLCs (Figure 4A). Other SLCs were not expressed in all of the tissue samples examined, but were detected, for example, in three out of five tissue samples. These SLCs were referred to as differentially experimented SLCs and are listed separately in Figure 4B. In the RNAseq data, additional 121–126 SLCs were differentially expressed in the duodenum tissue samples (Figure 4B). While Caco-2 cells expressed only 71–115 additional SLCs, ODMs and organoids expressed another 101–125 and 101–112 SLCs, respectively (Figure 4B). In contrast, the DNA microarray data detected 20 additional SLCs in duodenum tissue and 21 in ODMs and organoids, whereas Caco-2 cells had 27 additional SLCs. However, these data suggest that ODMs reflect the expression of SLCs of duodenal tissue well. Furthermore, the big variance within Caco-2 cells as well as within ODMs suggests that cultivation conditions may influence the expression of SLCs in both Caco-2 and ODMs.
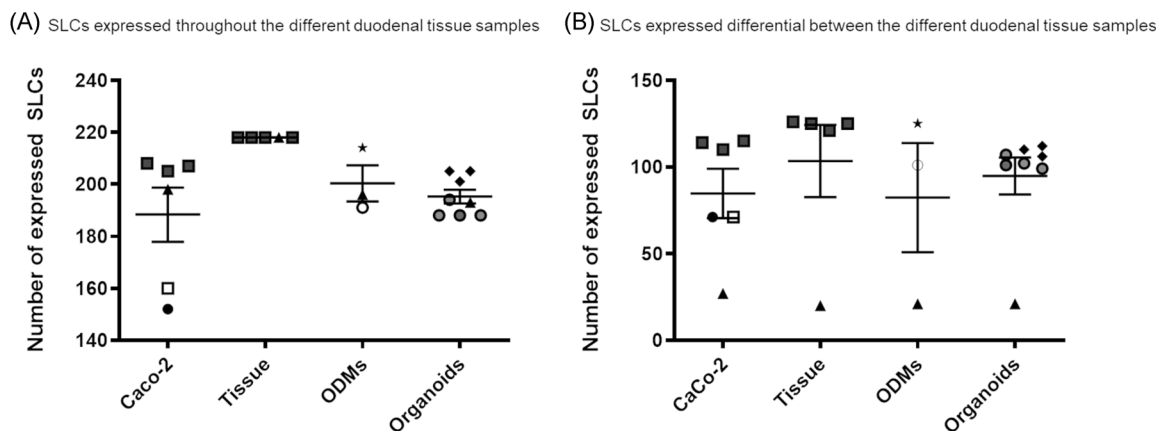
FIGURE 4 Comparison of transcriptomic data for SLC transporters in Caco-2 cells, duodenal tissue, organoids, and ODMs based on own and sequencing data in the literature. Comparison between the different groups indicated that SLC expression in ODMs and organoids was more like the *in vivo* situation than in Caco-2 cells. (A) 218 SLCs ($n = 5$) were expressed in all duodenal tissue samples, while ODMs expressed 191–214 ($n = 3$) SLCs, and organoids expressed 188–205 ($n = 8$) of these 218 SLCs. Caco-2 cells expressed 152–208 SLCs of 218 ($n = 8$). (B) Differentially expressed SLCs within duodenal tissue samples (20–116, $n = 5$), ODMs (21–125, $n = 3$), organoids (21–112; $n = 8$), and Caco-2 (27–115; $n = 6$). Each symbol presents one dataset: gray square ■ = GSE156453,[39] white square □ = Ma'ayeh *et al.*;[44] black circle ● = GSE164334,[38] black triangle ▲ = GSE160695,[43] white circle ○ = GSE163706,[42] black square ◆ = GSE127938,[40] gray circle ● = GSE167286,[41] black star ★ = own data[15] (values are shown as mean ± SEM)

TABLE 2 TJ morphometric analysis of freeze-fracture electron microscopy data

	N	Strands	TJ depth (nm)	Strand density (x/μm)	Breaks (x/μm single strand)
ODMs	52	4.58 ± 0.21	256.35 ± 16.30	17.85 ± 1.40	0.02 ± 0.02
Duodenal tissue	65	4.60 ± 0.14	250.77 ± 10.66	18.34 ± 0.96	0.02 ± 0.02
Caco-2	52	4.35 ± 0.28	258.17 ± 25.64	16.83 ± 1.99	0.07 ± 0.03

Stimulation of anion secretion with prostaglandin E2 and theophylline led to an increase in Cl⁻ secretion in ODMs, which indicated that ion transporters were not only expressed but were also functional. Treatment with a specific inhibitor for the Na-K-Cl cotransporter (NKCC1/SLC12A2), bumetanide, showed that this transporter was functional in ODMs (Figure S2A). To further compare different culture conditions, experiments to determine anion secretion and NKCC1/SLC12A2 activity were performed on ODMs as used in all other experiments in comparison to ODMs cultured as ALI. Here, treatment with bumetanide had no effect under ALI conditions, indicating inactivity of NKCC1/SLC12A2 in those cultures underlining again that culture conditions are of great importance.

Ultrastructural appearance of the TJ network

Besides the general expression profiles of TJ proteins, TJ ultrastructures were analyzed employing freeze-fracture electron microscopy. While, in general, the number of horizontally orientated strands and their distribution of occurrence, as well as the meshwork depth and resulting strand densities, were not different between Caco-2 cells, duodenal tissue, and ODM (Table 2), parameters of the strand appearance showed slight differences. Caco-2 cells tended to have higher strand break numbers and more often particle type and curved strands than the duodenal tissue. In contrast, the TJ strand appearance of ODMs did not differ at all from that of duodenal tissue (Figure 5).

Characterization of barrier properties

Although the TER already gives a rough impression of barrier functionality of developed ODMs, it gives no insight into specific properties of this barrier. Employing one-path impedance spectroscopy (Figure 6A), it was revealed that ODMs had very similar epithelial resistances (R^{epi}) as duodenal biopsies, while Caco-2 cells, which already had higher TER values, had eight times higher R^{epi} values than the biopsies. As cell lines do not possess subepithelial tissues, R^{sub} of the Caco-2 cells was reflecting the resistance of the filter support, which was 13.5 ± 1.8 Ω·cm². For ODMs, R^{sub} was formed not only by the filter support, but also by the Matrigel layer, leading to values similar to the subepithelial barrier of the biopsies and thus again seemed to be a good model for the tissue.

Further differentiation of R^{epi} into paracellular resistance (R^{para}) and transcellular resistance (R^{trans}) using two-path impedance
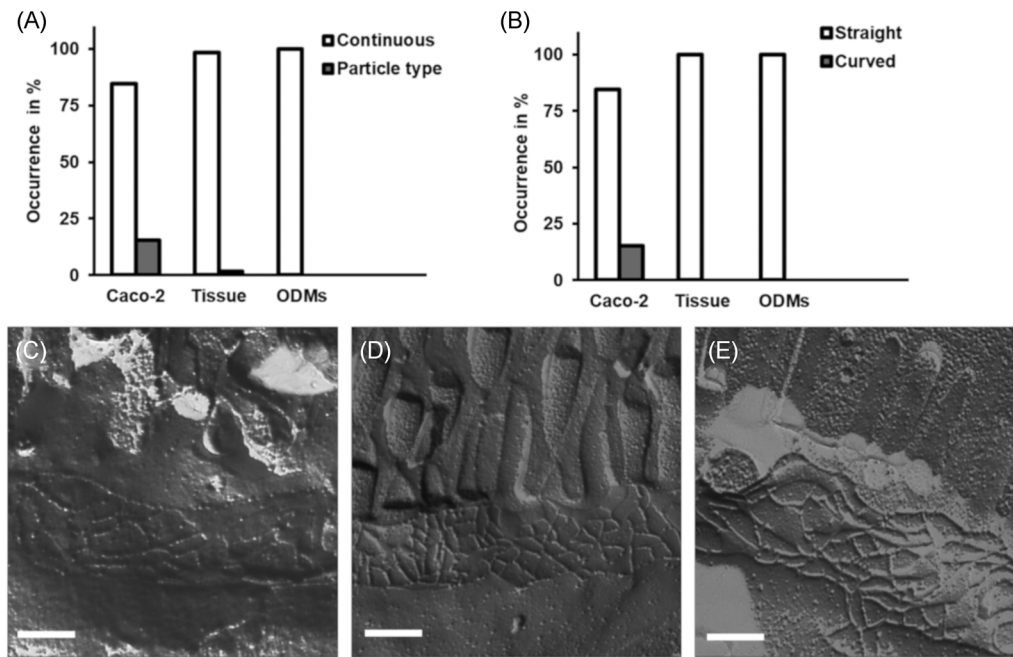
FIGURE 5 Ultrastructural appearance of the TJ of ODMs, human duodenal tissue, and Caco-2 cells. (A) Occurrence of particle type and continuous strands. In Caco-2 cells, the occurrence of particle-type strands was increased, while in tissue, this occurred sparsely and was not detected in ODMs. (B) Occurrence of straight and curved strands. Predominantly, straight TJ networks were found. However, in Caco-2 cells, a certain amount of curved TJs was detected. (C) Representative EM image of Caco-2 cells. (D) Representative EM image of human duodenal tissue. (E) Representative EM image of ODMs (bar = 200 nm)
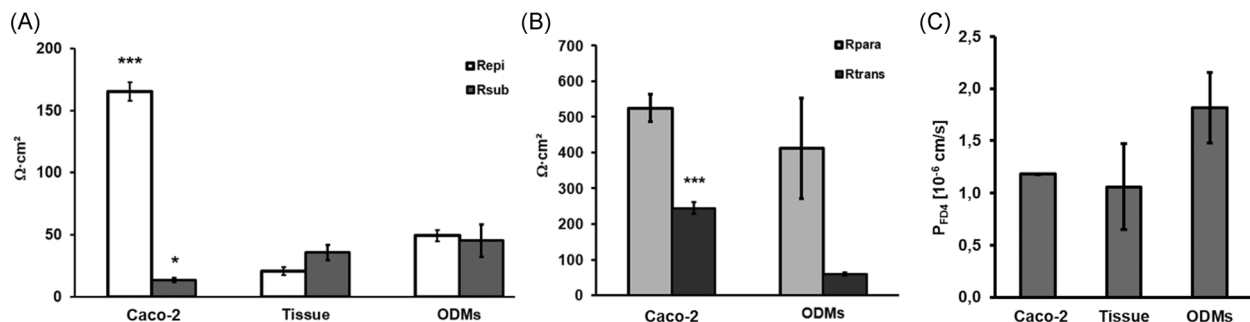

FIGURE 6 Functional analysis of ODMs, human duodenal tissue, and Caco-2 cells. (A) One-path impedance spectroscopic analysis. Caco-2 cells possessed higher epithelial resistance (R^{epi}) but lower subepithelial resistance (R^{sub}) than ODMs and duodenal tissue, which were both comparable to each other ($*p < 0.05$; $***p < 0.001$; $n = 5, 4, 4$). (B) Two-path impedance spectroscopic analysis. The higher R^{epi} of Caco-2 cells was based on increased transcellular resistance (R^{trans}) compared to ODMs, while paracellular resistance was similar to each other (R^{para}; $***p < 0.001$; $n = 5, 4, 4$). (C) Permeability for FITC-Dextran 4 kDa (P_{FD4}) was similar between Caco-2 ($1.18 \pm 0.003 \times 10^{-6}$ cm/s, $n = 16$), tissue ($1.06 \pm 0.41 \times 10^{-6}$ cm/s, $n = 5$), and ODMs ($1.82 \pm 0.34 \times 10^{-6}$ cm/s, $n = 4$), indicating that both barrier models Caco-2 and ODMs were sufficient to analyze paracellular barrier properties

revealed that the higher R^{epi} in Caco-2 cells was not due to an increase in R^{para} but due to a higher R^{trans} (Figure 6B), which means that Caco-2 cells might be still a good model for the epithelial barrier properties formed by TJs but may not possess all transcellular-resistance properties. An increased R^{trans} reflects a reduced transcellular ion transport in the Caco-2 cells, which indeed might be assumed to be lower when taking the reduced expression profile of SLCs in account that were observed in the comparison of transcriptomic data.

In sum, for ODMs, the impedance spectroscopic data supported that they reflected the trans- and paracellular barrier of the duodenal tissue well and that also the subepithelial barrier formed by the filter supports and Matrigel mimicked general subepithelial barrier properties of the tissue.

Paracellular fluxes

To further compare the paracellular barrier, permeability for macromolecules was determined using FITC-labeled Dextran with a molecular weight of 4 kDa (FD4). Caco-2, ODMs, and tissues had comparable permeabilities for FD4 (P_{FD4}) ranging between 1.0×10^{-6} cm/s and 2.0×10^{-6} cm/s (Figure 6C). These results emphasized that Caco-2 as well as ODMs were suitable models of the paracellular barrier in the context of macromolecule passage.

DISCUSSION

Researchers are continuously looking for better models to investigate their research target. To explore the intestinal barrier, either epithelial tissue from human biopsies or cell cultures are used. Recent developments introduced organoids as new models reflecting many properties of the tissues they are originating from. However, three-dimensional culture of these organoid models leads to some limitations in analyzing barrier properties and provides only limited access to the apical surface. ODMs were thus the next step to allow further analyses. In this study, the duodenal ODM model is presented and tested for its comparability with native tissue in terms of barrier function, macromolecule permeability, and ion permeability as defined by trans- and paracellular properties that are determined by TJ proteins and expression of SLCs.

With the SM/SM conditions, ODMs grew to confluent monolayers with stable TER, which is essential to study barrier function. Further, the expressions of TJ proteins like CLDN1, CLDN2, and OCLN were seen in ODMs.[15] Here, we did not only check for the presence of these already published TJ proteins, but also for the expression and localization of other and typical duodenal TJ proteins, the expression and correct localization of which could be confirmed in the ODMs (Figure 2). For example, TRIC was located specifically at tricellular cell contacts at the apical side as expected,[49] while LSR expression was extended to the lateral membrane at tTJs and bTJs, which fits to the reports of Masuda *et al.*[50]

Ultrastructural analysis of TJs showed that ODMs, Caco-2, and native tissues formed comparable strands, though the number of strand breaks, appearance of particle type, and curved strands was tendentially higher in Caco-2 cells (Figure 5). Particle-type strands were discussed to be linked to high CLDN2 expression for a long time, but Rosenthal *et al.* found no changes upon transfection of CLDN2 in MDCK C7 cells.[51] However, it is still assumed that particle-type strands are more abundant in leaky tissues.[52] Another explanation for the regional appearance of particle-type strands in Caco-2 cells may be the heterogeneous differentiation within the monolayer. Caco-2 cells differentiate in a patchy and mosaic-like pattern after reaching confluence.[53] This means that 2-weeks old Caco-2 cells tend to be heterogeneously differentiated and become more homogeneously with time. However, even 3-week-old Caco-2 cells have areas with distinct differences, which might cause the locational appearance of particle-type strands. Curved strands are associated with high CLDN3

and CLDN4 expression,[54,55] but the impact of particle-type strands and curved strands on the paracellular barrier function is not known so far. The occurrence of CLDN3- and CLDN4-rich region might be assumed in Caco-2 cells to be again linked to regional differentiation differences.

Quantification of TJ proteins using western blotting indicated that ODMs have a more similar TJ protein expression profile to native tissues than the Caco-2 cells (Figure 3). For example, the expression for CLDN2, TRIC, and OCLN was significantly higher in Caco-2 cells, while tissues had a significantly higher expression of CLDN7 compared with Caco-2 and ODMs. It was found that different cell types have a heterogeneous expression of TJ proteins and that in particular, CLDN2, OCLN, and TRIC are abundantly expressed in intestinal stem cells and Paneth cells, while CLDN7, on the other hand, is most abundantly expressed in enterocytes.[29] This suggests that ODMs and tissues have similar cell composition, and the SM/SM condition indeed leads to partial differentiation of the monolayers, as shown by the RT-qPCR results for different cell-type markers (Figure 1B), although tissues may have more differentiated enterocytes, as indicated by the high expression of CLDN7. CLDN7 is known not only to play a role in TJs but also to be important for differentiation and stem cell self-renewal.[56] These results further demonstrate that medium conditions may have a great influence and need to be carefully controlled, as they have an impact on cell differentiation, and thereby, also affect the composition of the TJ proteins. This is not only true for the medium condition but also for the overall condition, as mentioned here. ALI cultures showed no NKCC1/SLC12A2-specific ion transport (Figure S2), while in ODMs, this was measurable and could be inhibited, suggesting the inactivity of this transporter under ALI conditions. As the NKCC1/SLC12A2 is mainly associated with crypts, this could also point toward a more villus-like cellular make-up of the ODMs when not apically facing an ALI and thus, ALI cultures do not reflect well the physiological environmental conditions the duodenal tissue is exposed to. In conclusion, culturing conditions need to be wisely chosen to result in a proper model to experimental need.

Notwithstanding, ODMs appear as suitable model to investigate the TJ barrier, most important is the physiological function. As mentioned, confluency and a stable TER are essential features, which describe only very basic properties of the barrier by reflecting general ion permeabilities. With TER measurements, one cannot distinguish between epithelial and subepithelial barrier or trans- and paracellular barrier. This is possible by using one- or two-path impedance measurements, respectively. One-path impedance measurements showed much higher epithelial resistance of Caco-2 cells compared to tissue, while ODMs had properties similar to the tissue (Figure 6A). The two-path impedance data revealed that high epithelial resistance of Caco-2 cells was not caused by a higher paracellular resistance (TJs) but a higher TER (Figure 6B). This suggests missing properties of transporters, which fits to the results of the transcriptomic data, where Caco-2 cells tended to express less SLCs compared to ODMs and tissue. As R^{trans} reflects the transcellular ion transport, differently differentiated Caco-2 cells can be assumed to have also different R^{trans} values depending on the respective expression profiles and transport activity

of SLCs. Different SLC expressions between different publications within Caco-2 and ODMs imply that the culture conditions might also have an impact. It is already known that properties of Caco-2 differ between different laboratories.[6] However, in conclusion, the Caco-2 model might be still a good model for the general paracellular barrier properties, and ODMs reflect not only these but also transcellular properties in way comparable to the originating duodenal tissue.

The still in most parts comparable TJ protein expression and TJ appearance also supports similar paracellular barrier properties for both models. Besides, ion permeability also permeability for macromolecules was analyzed using FITC-dextran 4kDa (FD4), a typical paracellular flux marker, and confirmed similar permeability for macromolecules in Caco-2, ODMs, and tissues (Figure 6C).

However, in the work of Yamashita *et al.*,[43] ODMs were tested for their ability as a pharmacological model focusing on the metabolic activity of ODMs. Comparing gene expressions and activities of transporters important for drug metabolism like cytochrome P450 enzymes (e.g., CYP 3A4) and other apical (e.g., breast cancer-resistance protein) as well as basolateral (e.g., multidrug-resistance protein 3) transporters, it was revealed that ODMs were more similar to the adult duodenal tissue than Caco-2 cells, which confirms our finding that Caco-2 cells can only be used for transcellular investigations to a limited extent. Thus, both models have their advantages and drawbacks; whereas, Caco-2 cells are less labor- and cost-intensive and, therefore, might be the more robust model in most labs, ODMs may better reflect the different donor properties, which can help to identify patient-specific characteristics. Depending on the actual question, one or the other model may be favored. For example, in infection studies using *G. duodenalis*, scientists struggled with the Caco-2 model because it produced conflicting results,[57] and Caco-2 cells did not seem to tolerate the *Giardia* medium used for axenic culture.[58] Using ODMs, these problems were overcome, and intestinal cells were successfully infected allowing to study the interaction between *G. duodenalis* and the intestinal epithelium.[15]

In conclusion, the ODM model allows to study aspects of the duodenum that might not be solved using common cell cultures like Caco-2. They well-reflect the properties of their origin when cultured under optimized and standardized conditions in a reproducible way. They can not only be used to analyze trans- and paracellular barrier properties but also cell type-specific features as they are found in the duodenum. Furthermore, culture of organoids in a two-dimensional monolayer is just the start for developing even more realistic models of the intestine, for example, cocultures with apically exposed microbiota or basally added immune cells or subepithelial tissues of interest.

COMPETING INTERESTS

The authors declare no competing interests.

AUTHOR CONTRIBUTIONS

S.M.K. and F.W.: conception and design; S.M.K., F.W., D.H., M.K., and M.S.: acquisition of data; S.M.K. and F.W.: analysis and interpretation of data; S.M.K., F.W., and D.H.: participated in drafting the manuscript; S.M.K., F.W., D.H., C.K., J.D.S., and M.S. revising intellectual content. All authors have read and agreed to the published version of the manuscript.

ORCID

Franziska Weiß https://orcid.org/0000-0002-5069-9628
David Holthaus https://orcid.org/0000-0002-7012-5605
Martin Kraft https://orcid.org/0000-0002-6048-2959
Christian Klotz https://orcid.org/0000-0003-2609-9654
Martina Schneemann https://orcid.org/0000-0002-7900-1879
Jörg D. Schulzke https://orcid.org/0000-0001-9947-5521
Susanne M. Krug https://orcid.org/0000-0002-1293-2484

REFERENCES

1. Haber, A. L., Biton, M., Rogel, N., Herbst, R. H., Shekhar, K., Smillie, C., Burgin, G., Delorey, T. M., Howitt, M. R., Katz, Y., Tirosh, I., Beyaz, S., Dionne, D., Zhang, M., Raychowdhury, R., Garrett, W. S., Rozenblatt-Rosen, O., Shi, H. N., Yilmaz, O., … Regev, A. (2017). A single-cell survey of the small intestinal epithelium. *Nature*, *551*, 333–339.
2. Blanpain, C., Horsley, V., & Fuchs, E. (2007). Epithelial stem cells: Turning over new leaves. *Cell*, *128*, 445–458.
3. Beumer, J., & Clevers, H. (2021). Cell fate specification and differentiation in the adult mammalian intestine. *Nature Reviews Molecular Cell Biology*, *22*, 39–53.
4. Gross, D., & Tolba, R. H. (2015). Ethics in animal-based research. *European Surgical Research*, *55*, 43–57.
5. Barrett, K. E. (1993). Positive and negative regulation of chloride secretion in T84 cells. *American Journal of Physiology*, *265*(Pt 1), C859–C868.
6. Sambuy, Y., De Angelis, I., Ranaldi, G., Scarino, M. L., Stammati, A., & Zucco, F. (2005). The Caco-2 cell line as a model of the intestinal barrier: Influence of cell and culture-related factors on Caco-2 cell functional characteristics. *Cell Biology and Toxicology*, *21*, 1–26.
7. Oltra-Noguera, D., Mangas-Sanjuan, V., Centelles-Sangüesa, A., Gonzalez-Garcia, I., Sanchez-Castaño, G., Gonzalez-Alvarez, M., Casabo, V.-G., Merino, V., Gonzalez-Alvarez, I., & Bermejo, M. (2015). Variability of permeability estimation from different protocols of subculture and transport experiments in cell monolayers. *Journal of Pharmacological and Toxicological Methods*, *71*, 21–32.
8. Sun, H., Chow, E. C., Liu, S., Du, Y., & Pang, K. S. (2008). The Caco-2 cell monolayer: Usefulness and limitations. *Expert Opinion on Drug Metabolism & Toxicology*, *4*, 395–411.
9. Grossmann, J., Walther, K., Artinger, M., Kiessling, S., Steinkamp, M., Schmautz, W.-K., Stadler, F., Bataille, F., Schultz, M., Schölmerich, J., &

Rogler, G. (2003). Progress on isolation and short-term *ex-vivo* culture of highly purified non-apoptotic human intestinal epithelial cells (IEC). *European Journal of Cell Biology*, 82, 262–270.

10. Sato, T., Vries, R. G., Snippert, H. J., Van De Wetering, M., Barker, N., Stange, D. E., Van Es, J. H., Abo, A., Kujala, P., Peters, P. J., & Clevers, H. (2009). Single Lgr5 stem cells build crypt–villus structures *in vitro* without a mesenchymal niche. *Nature*, 459, 262–265.

11. Merker, S. R., Weitz, J., & Stange, D. E. (2016). Gastrointestinal organoids: How they gut it out. *Developmental Biology*, 420, 239–250.

12. Seidlitz, T., Merker, S. R., Rothe, A., Zakrzewski, F., Von Neubeck, C., Grützmann, K., Sommer, U., Schweitzer, C., Schölch, S., Uhlemann, H., Gaebler, A.-M., Werner, K., Krause, M., Baretton, G. B., Welsch, T., Koo, B.-K., Aust, D. E., Klink, B., Weitz, J., & Stange, D. E. (2019). Human gastric cancer modelling using organoids. *Gut*, 68, 207–217.

13. Beumer, J., & Clevers, H. (2016). Regulation and plasticity of intestinal stem cells during homeostasis and regeneration. *Development (Cambridge, England)*, 143, 3639–3649.

14. Schlaermann, P., Toelle, B., Berger, H., Schmidt, S. C., Glanemann, M., Ordemann, J., Bartfeld, S., Mollenkopf, H. J., & Meyer, T. F. (2016). A novel human gastric primary cell culture system for modelling *Helicobacter pylori* infection *in vitro*. *Gut*, 65, 202–213.

15. Holthaus, D., Kraft, M. R., Krug, S. M., Wolf, S., Müller, A., Betancourt, E. D., Schorr, M., Holland, G., Knauf, F., Schulzke, J.-D., Aebischer, T., & Klotz, C. (2021). Dissection of barrier dysfunction in organoid-derived human intestinal epithelia induced by *Giardia duodenalis*. *Gastroenterology*, 162(3), 844–858.

16. D'aldebert, E., Quaranta, M., Sébert, M., Bonnet, D., Kirzin, S., Portier, G., Duffas, J.-P., Chabot, S., Lluel, P., Allart, S., Ferrand, A., Alric, L., Racaud-Sultan, C., Mas, E., Deraison, C., & Vergnolle, N. (2020). Characterization of human colon organoids from inflammatory bowel disease patients. *Frontiers in Cell and Developmental Biology*, 8, 363.

17. Nakamura, T. (2019). Recent progress in organoid culture to model intestinal epithelial barrier functions. *International Immunology*, 31, 13–21.

18. Sato, T., Stange, D. E., Ferrante, M., Vries, R. G. J., Van Es, J. H., Van Den Brink, S., Van Houdt, W. J., Pronk, A., Van Gorp, J., Siersema, P. D., & Clevers, H. (2011). Long-term expansion of epithelial organoids from human colon, adenoma, adenocarcinoma, and Barrett's epithelium. *Gastroenterology*, 141, 1762–1772.

19. Kozuka, K., He, Y., Koo-McCoy, S., Kumaraswamy, P., Nie, B., Shaw, K., Chan, P., Leadbetter, M., He, L., Lewis, J. G., Zhong, Z., Charmot, D., Balaa, M., King, A. J., Caldwell, J. S., & Siegel, M. (2017). Development and characterization of a human and mouse intestinal epithelial cell monolayer platform. *Stem Cell Reports*, 9(6), 1976–1990.

20. Vandussen, K. L., Marinshaw, J. M., Shaikh, N., Miyoshi, H., Moon, C., Tarr, P. I., Ciorba, M. A., & Stappenbeck, T. S. (2015). Development of an enhanced human gastrointestinal epithelial culture system to facilitate patient-based assays. *Gut*, 64, 911–920.

21. Moon, C., Vandussen, K. L., Miyoshi, H., & Stappenbeck, T. S. (2014). Development of a primary mouse intestinal epithelial cell monolayer culture system to evaluate factors that modulate IgA transcytosis. *Mucosal Immunology*, 7, 818–828.

22. Moorefield, E. C., Blue, R. E., Quinney, N. L., Gentzsch, M., & Ding, S. (2018). Generation of renewable mouse intestinal epithelial cell monolayers and organoids for functional analyses. *BMC Cell Biology*, 19, 15.

23. Holthaus, D., Delgado-Betancourt, E., Aebischer, T., Seeber, F., & Klotz, C. (2020). Harmonization of protocols for multi-species organoid platforms to study the intestinal biology of *Toxoplasma gondii* and other Protozoan infections. *Frontiers in Cellular and Infection Microbiology*, 10, 610368.

24. Warschkau, D., Delgado-Betancourt, E., Holthaus, D., Müller, A., Kliem, G., Krug, S., Schulzke, J.-D., Aebischer, T., Klotz, C., & Seeber, F. (2022). From 3D to 2D: Harmonization of protocols for two-dimensional cultures on cell culture inserts of intestinal organoids from various species. *Bio-Protocol*, 12(2), e4295.

25. Morita, K., Furuse, M., Fujimoto, K., & Tsukita, S. (1999). Claudin multigene family encoding four-transmembrane domain protein components of tight junction strands. *Proceedings of the National Academy of Sciences of the United States of America*, 96, 511–516.

26. Raleigh, D. R., Marchiando, A. M., Zhang, Y., Le, S., Sasaki, H., Wang, Y., Long, M., & Turner, J. R. (2010). Tight junction-associated MARVEL proteins marveld3, tricellulin, and occludin have distinct but overlapping functions. *Molecular Biology of the Cell*, 21, 1200–1213.

27. Higashi, T., Tokuda, S., Kitajiri, S.-I., Masuda, S., Nakamura, H., Oda, Y., & Furuse, M. (2013). Analysis of the 'angulin' proteins LSR, ILDR1 and ILDR2–tricellulin recruitment, epithelial barrier function and implication in deafness pathogenesis. *Journal of Cell Science*, 126(Pt 4), 966–977.

28. Stevenson, B. R., Siliciano, J. D., Mooseker, M. S., & Goodenough, D. A. (1986). Identification of ZO-1: A high molecular weight polypeptide associated with the tight junction (zonula occludens) in a variety of epithelia. *Journal of Cell Biology*, 103, 755–766.

29. Pearce, S. C., Al-Jawadi, A., Kishida, K., Yu, S., Hu, M., Fritzky, L. F., Edelblum, K. L., Gao, N., & Ferraris, R. P. (2018). Marked differences in tight junction composition and macromolecular permeability among different intestinal cell types. *BMC Biology*, 16, 19.

30. Bartfeld, S., Bayram, T., Van De Wetering, M., Huch, M., Begthel, H., Kujala, P., Vries, R., Peters, P. J., & Clevers, H. (2015). *In vitro* expansion of human gastric epithelial stem cells and their responses to bacterial infection. *Gastroenterology*, 148, 126–136.e6.

31. Vandussen, K. L., Sonnek, N. M., & Stappenbeck, T. S. (2019). L-WRN conditioned medium for gastrointestinal epithelial stem cell culture shows replicable batch-to-batch activity levels across multiple research teams. *Stem Cell Research*, 37, 101430.

32. Kim, K.-A., Kakitani, M., Zhao, J., Oshima, T., Tang, T., Binnerts, M., Liu, Y., Boyle, B., Park, E., Emtage, P., Funk, W. D., & Tomizuka, K. (2005). Mitogenic influence of human R-spondin1 on the intestinal epithelium. *Science*, 309, 1256–1259.

33. Heijmans, J., Van Lidth De Jeude, J. F., Koo, B.-K., Rosekrans, S. L., Wielenga, M. C. B., Van De Wetering, M., Ferrante, M., Lee, A. S., Onderwater, J. J. M., Paton, J. C., Paton, A. W., Mommaas, A. M., Kodach, L. L., Hardwick, J. C., Hommes, D. W., Clevers, H., Muncan, V., & Van Den Brink, G. R. (2013). ER stress causes rapid loss of intestinal epithelial stemness through activation of the unfolded protein response. *Cell Reports*, 3, 1128–1139.

34. Yin, X., Farin, H. F., Van Es, J. H., Clevers, H., Langer, R., & Karp, J. M. (2014). Niche-independent high-purity cultures of Lgr5+ intestinal stem cells and their progeny. *Nature Methods*, 11, 106–112.

35. Miyoshi, H., Vandussen, K. L., Malvin, N. P., Ryu, S. H., Wang, Y., Sonnek, N. M., Lai, C.-W., & Stappenbeck, T. S. (2017). Prostaglandin E2 promotes intestinal repair through an adaptive cellular response of the epithelium. *Embo Journal*, 36, 5–24.

36. Wang, Y., Chiang, I.-L., Ohara, T. E., Fujii, S., Cheng, J., Muegge, B. D., Ver Heul, A., Han, N. D., Lu, Q., Xiong, S., Chen, F., Lai, C.-W., Janova, H., Wu, R., Whitehurst, C. E., Vandussen, K. L., Liu, T.-C., Gordon, J. I., Sibley, L. D., & Stappenbeck, T. S. (2019). Long-term culture captures injury-repair cycles of colonic stem cells. *Cell*, 179, 1144–1159.e15.

37. Engle, M. J., Goetz, G. S., & Alpers, D. H. (1998). Caco-2 cells express a combination of colonocyte and enterocyte phenotypes. *Journal of Cellular Physiology*, 174, 362–369.

38. He, Y., Yin, X., Dong, J., Yang, Q., Wu, Y., & Gong, Z. (2021). Transcriptome analysis of Caco-2 cells upon the exposure of mycotoxin deoxynivalenol and its acetylated derivatives. *Toxins (Basel)*, 167, 13.

39. Takayama, K., Ito, K., Matsui, A., Yamashita, T., Kawakami, K., Hirayama, D., Kishimoto, W., Nakase, H., & Mizuguchi, H. (2021). *In vivo* gene expression profile of human intestinal epithelial cells: From the viewpoint of drug metabolism and pharmacokinetics. *Drug Metabolism and Disposition*, 49, 221–232.

40. Kayisoglu, O., Weiss, F., Niklas, C., Pierotti, I., Pompaiah, M., Wallaschek, N., Germer, C.-T., Wiegering, A., & Bartfeld, S. (2021). Location-specific cell identity rather than exposure to GI microbiota defines many innate immune signalling cascades in the gut epithelium. *Gut*, *70*, 687–697.

41. Gu, W., Wang, H., Huang, X., Kraiczy, J., Singh, P. N. P., Ng, C., Dagdeviren, S., Houghton, S., Pellon-Cardenas, O., Lan, Y., Nie, Y., Zhang, J., Banerjee, K. K., Onufer, E. J., Warner, B. W., Spence, J., Scherl, E., Rafii, S., Lee, R. T., Verzi, M. P., Redmond, D., Longman, R., Helin, K., Shivdasani, R. A., & Zhou, Q. (2022). SATB2 preserves colon stem cell identity and mediates ileum-colon conversion via enhancer remodeling. *Cell Stem Cell*, *29*, 101–115.e10.

42. Sugimoto, S., Kobayashi, E., Fujii, M., Ohta, Y., Arai, K., Matano, M., Ishikawa, K., Miyamoto, K., Toshimitsu, K., Takahashi, S., Nanki, K., Hakamata, Y., Kanai, T., & Sato, T. (2021). An organoid-based organ-repurposing approach to treat short bowel syndrome. *Nature*, *592*, 99–104.

43. Yamashita, T., Inui, T., Yokota, J., Kawakami, K., Morinaga, G., Takatani, M., Hirayama, D., Nomoto, R., Ito, K., Cui, Y., Ruez, S., Harada, K., Kishimoto, W., Nakase, H., & Mizuguchi, H. (2021). Monolayer platform using human biopsy-derived duodenal organoids for pharmaceutical research. *Molecular Therapy – Methods & Clinical Development*, *22*, 263–278.

44. Ma'ayeh, S. Y., Knörr, L., Sköld, K., Garnham, A., Ansell, B. R. E., Jex, A. R., & Svärd, S. G. (2018). Responses of the differentiated intestinal epithelial cell line Caco-2 to infection with the *Giardia* intestinalis GS isolate. *Frontiers in Cellular and Infection Microbiology*, *8*, 244.

45. Zeissig, S., Burgel, N., Gunzel, D., Richter, J., Mankertz, J., Wahnschaffe, U., Kroesen, A. J., Zeitz, M., Fromm, M., & Schulzke, J.-D. (2007). Changes in expression and distribution of claudin 2, 5 and 8 lead to discontinuous tight junctions and barrier dysfunction in active Crohn's disease. *Gut*, *56*, 61–72.

46. Stevenson, B. R., Anderson, J. M., Goodenough, D. A., & Mooseker, M. S. (1988). Tight junction structure and ZO-1 content are identical in two strains of Madin–Darby canine kidney cells which differ in transepithelial resistance. *Journal of Cell Biology*, *107*(6 Pt 1), 2401–2408.

47. Krug, S. M., Fromm, M., & Günzel, D. (2009). Two-path impedance spectroscopy for measuring paracellular and transcellular epithelial resistance. *Biophysical Journal*, *97*, 2202–2211.

48. Yen, F. T., Masson, M., Clossais-Besnard, N., André, P., Grosset, J.-M., Bougueleret, L., Dumas, J.-B., Guerassimenko, O., & Bihain, B. E. (1999). Molecular cloning of a lipolysis-stimulated remnant receptor expressed in the liver. *Journal of Biological Chemistry*, *274*, 13390–13398.

49. Ikenouchi, J., Furuse, M., Furuse, K., Sasaki, H., Tsukita, S., & Tsukita, S. (2005). Tricellulin constitutes a novel barrier at tricellular contacts of epithelial cells. *Journal of Cell Biology*, *171*, 939–945.

50. Masuda, S., Oda, Y., Sasaki, H., Ikenouchi, J., Higashi, T., Akashi, M., Nishi, E., & Furuse, M. (2011). LSR defines cell corners for tricellular tight junction formation in epithelial cells. *Journal of Cell Science*, *124*(Pt 4), 548–555.

51. Rosenthal, R., Milatz, S., Krug, S. M., Oelrich, B., Schulzke, J.-D., Amasheh, S., Günzel, D., & Fromm, M. (2010). Claudin-2, a component of the tight junction, forms a paracellular water channel. *Journal of Cell Science*, *123*(Pt 11), 1913–1921.

52. Fromm, M., Piontek, J., Rosenthal, R., Günzel, D., & Krug, S. M. (2017). Tight junctions of the proximal tubule and their channel proteins. *Pflugers Archiv: European Journal of Physiology*, *469*, 877–887.

53. Vachon, P. H., & Beaulieu, J.-F. (1992). Transient mosaic patterns of morphological and functional differentiation in the Caco-2 cell line. *Gastroenterology*, *103*, 414–423.

54. Milatz, S., Krug, S. M., Rosenthal, R., Günzel, D., Müller, D., Schulzke, J.-D., Amasheh, S., & Fromm, M. (2010). Claudin-3 acts as a sealing component of the tight junction for ions of either charge and uncharged solutes. *Biochimica et Biophysica Acta*, *1798*, 2048–2057.

55. Van Itallie, C., Rahner, C., & Anderson, J. M. (2001). Regulated expression of claudin-4 decreases paracellular conductance through a selective decrease in sodium permeability. *Journal of Clinical Investigation*, *107*, 1319–1327.

56. Xing, T., Benderman, L. J., Sabu, S., Parker, J., Yang, J., Lu, Q., Ding, L., & Chen, Y.-H. (2020). Tight junction protein claudin-7 is essential for intestinal epithelial stem cell self-renewal and differentiation. *Cellular and Molecular Gastroenterology and Hepatology*, *9*, 641–659.

57. Kraft, M. R., Klotz, C., Bücker, R., Schulzke, J.-D., Aebischer, T. (2017). *Giardia's* epithelial cell interaction *in vitro*: Mimicking asymptomatic infection? *Frontiers in Cellular and Infection Microbiology*, *7*, 421.

58. Nash, T. E. (2019). Long-term culture of *Giardia lamblia* in cell culture medium requires intimate association with viable mammalian cells. *Infection and Immunity*, *87*, e00639-19.

SUPPORTING INFORMATION

Additional supporting information can be found online in the Supporting Information section at the end of this article.